Corrections for Intensity Data in Energy-dispersive X-Ray Diffractometry of Liquids. Application to Carbon Tetrachloride

Keiko NISHIKAWA* and Takao IIJIMA
Department of Chemistry, Faculty of Science, Gakushuin University, Mejiro, Toshima-ku, Tokyo 171
(Received December 13, 1983)

The procedure of the analysis of the diffraction intensity of liquids obtained by the energy-dispersive method has been revised and improved. A new method for determining the energy spectrum of the primary beam is presented. The escape correction, the slit correction and the correction for multiple scattering have been newly applied. Scattering of X-rays from liquid CCl_4 has been measured and its structure function has been obtained by an improved procedure.

The intensity measurement of scattered X-rays by the use of energy-dispersive method has been carried out in various experiments since it was introduced by Giessen and Gordon.[1] In the energy-dispersive method, white X-rays are used as the primary beam and the scattered photons are detected and energy-analyzed by a solid state detector (SSD) connected with a multichannel pulse height analyzer (MCA). The energies of detected photons are distributed over the whole energy-region of the primary beam, so the scattering intensities of a certain range of the scattering parameters s, ($s=(4\pi\sin\theta/hc)E$, 2θ: scattering angle, E: photon energy), are accumulated in parallel.

This method has various advantages[2-4] over the conventional angle-dispersive method. However, the rather complex procedure of the data analysis is a drawback. The problems in the data analysis for quantitative intensity studies are as follows:

1) the determination of the properties of the primary beam, namely, the energy spectrum and the energy dependence of polarizaion of the primary beam,

2) the corrections for the effects originating from the detector, the slit system and the sample, namely, the escape correction when pure Ge or Ge(Li) detector is used, the slit correction and the absorption correction,

3) the correction for multiple scattering and the theoretical estimation of the intensity of Compton scattering.

Prober and Schultz performed the first quantitative measurement of the diffraction intensity from a sample which gives a halo pattern by the use of the energy-dispersive technique.[5] Three years later, Murata and one of the present authors (K. N.),[2] and Egami[3] reported the construction of their energy-dispersive diffractometers and the procedures of data analysis. In recent years, the energy-dispersive technique was also applied to the measurement of scattering intensities from gases.[6]

Prober and Schultz determined the energy spectrum of the primary beam by comparing the observed scattering intensity of the sample itself at high s-values, where the curve of the diffraction intensity is smooth without any particular structure, with the theoretical scattering intensity of mercury atoms.[5] However, they neglected the Compton shift in this procedure. This negligence seems to lead to a serious error. Egami followed the method by Prober and Schultz in determination of the primary energy spectrum, and developed this method considering the Compton shift.[3] For the determination of not only the primary energy spectrum but also the absorption coefficient of the sample, Egami proposed a self-consistent analysis.[3,4,7] However, it seems unreliable because too many parameters have to be determined simultaneously. Egami did not make the escape correction and the slit correction.

Murata and Nishikawa directly observed the energy spectrum of the primary beam by the use of the same slit system as in the measurement of scattered X-rays from samples, reducing the radiation intensity by decreasing the tube current to a few micro-amperes.[2] However, there has been anxiety about whether or not the decrease of the tube current produces distortion of the energy spectrum of the primary beam. In the data analysis of Ref. 2, the recoil factor for free electrons was used and the band-width ratio in the Compton shift was ignored. The polarization of the primary beam was neglected. Actually the effect has been found to be small in the energy region they used.

In the present paper, we report a procedure of improved data analysis of the energy-dispersive method and the structure function of liquid CCl_4 obtained by the improved procedure.

Experimental

Diffractometer. Since the main constitution of the apparatus is the same as that in Ref. 2, only the outline is given in the following. The geometry of the diffractometer is shown in Fig. 1. A horizontal goniometer system is adopted, in which an X-ray source and a detector are set in a horizontal plane. Although measurement by the energy-dispersive tech-

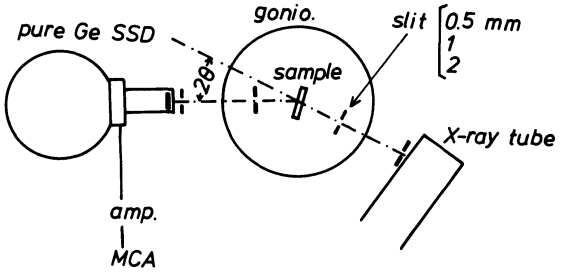

Fig. 1. Schematic diagram of the energy-dispersive diffractometer.

nique is carried out at a fixed scattering angle, such measurement must be repeated at different angles in order to cover a sufficiently wide region of s-space. To change the scattering angle, the X-ray tube is rotated around the vertical axis of the goniometer, which has a θ-2θ scanning system, while the detector (SSD) with a heavy cryostat is fixed.

A fine focus Phillips tube with a tungsten target is used, because strong white X-rays can be obtained without disturbance by characteristic X-rays, and the applicable power is large. The high voltage power supply for X-rays (Rigaku Denki Co.) is used. The stability of the high voltage is better than 0.1%. The X-ray tube is usually operated at 47.5 kV and 30 mA. The scattered X-rays are detected by a pure Ge SSD (ORTEC, Model 1513-10190). A pair of slits made of lead is used for both the incident and the detecting collimators. The separation of the two slits is about 150 mm. The width of the slit is varied: 0.5, 1, and 2 mm, and the height is 6 mm. The sample holder reported previously[8] is attached at the center of the goniometer. The transmission geometry is employed in order to make absorption correction easier.

Measurement of CCl_4. The diffracted X-ray photons from liquid CCl_4 at room temperature were collected at the scattering angles of 2θ=2.5, 4, 6, 10, 16, 28, 40, and 56°, by operating the X-ray tube at 47.5 kV and 30 mA. The spectrum in the energy-region 12—38 keV (λ=1.03—0.326 Å) is used for the analysis. The settings of 2θ=2.5, 4, 6, 10, 16, 28, 40, and 56° correspond to the regions of s=0.27—0.84, 0.42—1.34, 0.64—2.02 1.06—3.36, 1.69—5.36, 2.94—9.32, 4.16—13.18 and 5.71—18.09 Å^{-1}, respectively. In usual structure studies it is not necessary to measure the intensities at so many scattering angles. However, in the present experiment it is desired to obtain justification of a procedure of an analysis that includes several corrections. This is ascertained by checking the consistency of the data in the same s-regions which have been collected at different settings of the scattering angles and analyzed independently.

The scattering from Myler films, 5 μm thick, of the windows of the sample holder, was also measured. The measurement includes the scattering intensity from air, too. The thickness of the sample was 0.50 mm.

In order to obtain the relation of the photon energy *vs.* the channel number in the MCA, the fluorescent X-rays from Ba, Ag, Mo, Cu, and Cr were observed. The channel numbers of these peaks in the MCA were fitted to the energies of the corresponding characteristic X-rays by using a table by Bearden.[9] The linear relationship between the photon energy and the channel number is good.

The Properties of the Primary Beam

The Energy Spectrum of the Primary Beam. The energy spectrum of the primary beam was determined by measuring the scattering from air at low scattering angle with the same slit system and the same operating conditions of the tube as in the measurement of the sample. This method requires no particular preparation, because the diffraction measurement without the sample holder gives the scattering intensity from air. The scattering intensity of air at low scattering angles is strong enough to measure by the use of a usual sealed-off tube, because the effective volume of air which scatters X-rays is fairly large. In the analysis of the data of low scattering angles, it is permissible to neglect the Compton shift and the polarization of the primary beam. Moreover, the scattering amplitudes of light atoms such as N and O can be theoretically calculated with high accuracy.[10]

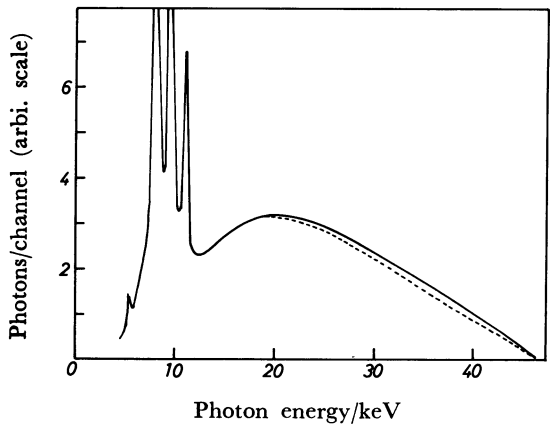

Fig. 2. The energy spectra of the primary beam. The solid curve is the spectrum determined by measuring scattering intensities of air. The broken curve is the one obtained by direct measurement by decreasing the tube current to a few micro-amperes.

The spectrum of the primary beam obtained from the scattering intensity of air is shown in Fig. 2, where it is compared with the spectrum measured directly at a tube current of a few micro-amperes. As is shown in Fig. 2, the intensity at high energy region obtained from air is stronger than that from the direct measurement. This seems to be caused by the difference between the amplitude of the ripples of the imperfectly smoothed voltage applied to the X-ray tube for the tube current of milli-amperes and that for the tube current of micro-amperes. In the former case the amplitude of the ripples is greater than that in the latter. The number of photons of radiated X-rays in a channel is not simply proportional to the applied voltage. So the intensity at the high energy region may become stronger in the case of the operation at milli-amperes. Another origin of the difference in the energy spectrum of the primary beam may be the difference of the size of the focus of the electron beam on the target.

The Polarization of the Primary Beam. It is known that the white X-ray radiation is polarized in the direction parallel to the electron beam at the high energy limit of the Bremsstrahlung spectrum.[11] The polarization $\Pi(E)$ of the primary beam is defined by

$$\Pi(E) = (I_{p,n}(E) - I_{p,p}(E))/(I_{p,n}(E) + I_{p,p}(E)), \quad (1)$$

where $I_{p,n}$ and $I_{p,p}$ are the intensities of the normal and parallel polarization components, respectively, with respect to the scattering plane. It is known that the polarization $\Pi(E)$ of white X-rays from a thin target is very large, and some experiments of such samples have been reported. However, there have been very few measurements for the polarization $\Pi(E)$ from such thick targets as those used in commercial sealed-off tubes. One recent example was the experiment carried out by Olsen *et al.*[12]

We also measured the polarization $\Pi(E)$ of our X-ray tube with a tungsten target (Phillips fine focus) at 47.5 kV. Two scattering intensities from silica glass were measured at a fixed scattering angle with

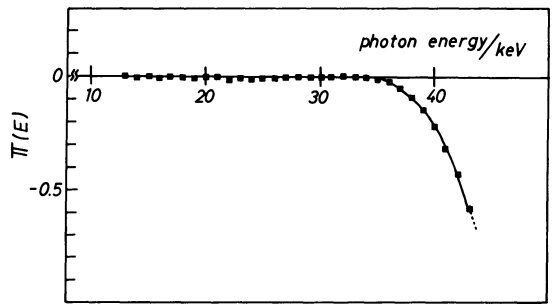

Fig. 3. The measured polarization $\Pi(E)$ of the used tungsten tube at 47.5 kV.

point focus collimators. One of them was the intensity measured in the ordinary condition where the X-ray tube was set on the scattering plane, and the other was that where the X-ray tube was set perpendicular to the scattering plane. From these two intensities, the polarization $\Pi(E)$ was obtained as shown in Fig. 3. The result is in fairly good agreement with that of Olsen *et al.*[12] However, the present result contains large uncertainties, because $\Pi(E)$ is computed from the differences of the two intensities which are nearly equal.

The $\Pi(E)$ amounts to almost -0.5 at the high energy limit, but up to the energy of 38 keV which is 0.8× (incident electron energy), absolute value of $\Pi(E)$ is below 0.1. So, in order to make the error caused by the polarization of the primary beam small, it is preferable to use the data whose energy region is below 0.8×(incident electron energy). By the use of this energy region, the errors due to the polarization contained in the data which are obtained at the scattering angle below 25° are less than 1%. But at high angles, for example, 2θ=56°, they amount to 5% if the polarization correction is not made. In our data, which are corrected by the use of the measured polarization, $\Pi(E)$, the estimated uncertainties are about 1% even at high scattering angles (2θ=40 and 56°).

In order to cancel the effect of polarization, Olsen *et al.*[12] and Egami[3] proposed the use of a diffractometer with an X-ray tube tilted away from the diffraction plane by 45°. In aperture collimator systems, this method may be used. However, it is not suitable in the case of slit systems, because the projection of the slit height on the scattering plane becomes large and the resolution of the scattering angle becomes low.

Correction for the Effects Originating from the Detector, the Slit System and the Sample

The Escape Correction. When a pure Ge or Li drifted Ge SSD is used, escape peaks are observed.[13] Some photons which come into the detector excite K electrons of Ge atoms and produce $K\alpha$ or $K\beta$ fluorescent X-rays characteristic of Ge. If the fluorescent X-ray photon is instantly re-absorbed in the crystal of the SSD, the output pulse height from the detector has a value corresponding to the energy of the original photon that entered the detector. However, if the fluorescent X-ray photon escapes from the detector

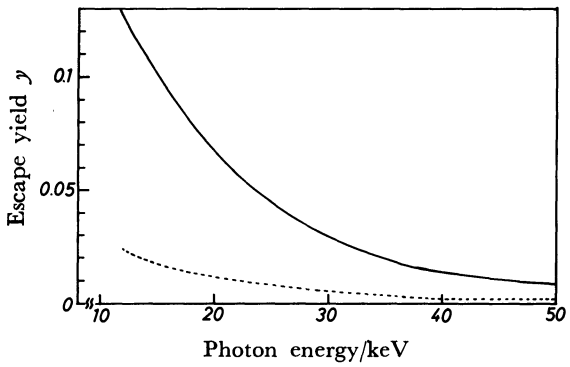

Fig. 4. The escape yield, $y(E)$, of the Ge SSD.[14] The solid curve is the yield for $K\alpha$ photons, and the broken curve for $K\beta$ photons.

crystal, the pulse height from the detector decreases to the value corresponding to the original photon energy minus E_k, the energy of Ge $K\alpha$ or $K\beta$ photons. Thus the number of photons counted at the energy E becomes less, and that at the energy $E-E_k$ becomes more, than the values they shoud be, where E_k is about 10 keV.

The yield of the escape, $y(E)$, of the Ge SSD used in the present work was measured by Mitsuhashi *et al.*, by the use of a single crystal of Si.[6,14] It is shown in Fig. 4.

With a little manipulation, we obtain the following formula for the true intensity I_0 at energy E:

$$I_0 = J_0 - \frac{y_1}{1-y_1}J_1 + \frac{y_1y_2}{(1-y_1)(1-y_2)}J_2 - \frac{y_1y_2y_3}{(1-y_1)(1-y_2)(1-y_3)}J_3 + \cdots\cdots \quad (\text{for } E<E_k) \quad (2)$$

and

$$I_0 = \frac{1}{1-y_0}\left[J_0 - \frac{y_1}{1-y_1}J_1 + \frac{y_1y_2}{(1-y_1)(1-y_2)}J_2 - \frac{y_1y_2y_3}{(1-y_1)(1-y_2)(1-y_3)}J_3 + \cdots\cdots\right] \quad (\text{for } E\geq E_k) \quad (3)$$

where J_n is the apparent intensity observed by the Ge SSD at the energy $E+nE_k$; y_n is the escape yield at the energy $E+nE_k$. The progression in Eq. 2 or 3 is terminated at the n-th term where the energy of $(E+(n+1)E_k)$ becomes for the first time greater than the high energy limit which is determined by the applied tube voltage. By the use of the measured values of y_n and J_n, we can make the escape correction with sufficient accuracy.

Slit Correction. The peaks and valleys of the observed intensity curve are smeared by the convolution due to the dispersion of the scattering angle, which is determined by the geometrical arrangement and widths of the slits. For liquid CCl_4, which gives a sharp peak at small s-values, the reduction of the peak height caused by this convolution is a serious problem.

According to the method of the slit correction in the experiment of small angle scattering[15] the deconvoluted intensity $I(s)$ is approximately given by

$$I(s) = 2\tilde{I}(s) - [\tilde{I}(s+\Delta s)+\tilde{I}(s-\Delta s)]/2, \quad (4)$$

where $\tilde{I}(s)$ is the observed intensity at s and Δs is the dispersion of the scattering parameter s, which is related to the angle dispersion ξ by the following formula:

$$\Delta s = \frac{4\pi}{hc} E \sin(\theta+\xi) - \frac{4\pi}{hc} E \sin\theta. \quad (5)$$

The parameter ξ is the dispersion of the angle caused by the width of slits. The values of ξ are estimated to be 0.125, 0.250, and 0.50° for the slits with the widths of 0.5, 1, and 2 mm, respectively, in the geometrical arrangement of the present work. The details of the estimation of ξ are given in Appendix 1. The first peak at $s \simeq 1.3 \text{Å}^{-1}$ for liquid CCl_4 becomes 5% higher than that without the slit correction, when the data were obtained at the scattering angle of $2\theta=6°$ and 0.5 mm slit systems with 150 mm separation were used.

Absorption Correction. The most important correction in energy-dispersive diffractometry is the absorption correction, because the linear absorption coefficient, μ, changes to a great extent with the energy of the X-rays. The values of $\mu(E)$ were experimentally determined from the measurements of the transmittance of the sample at $\theta=0°$ with the primary beam. The tube was operated at a few micro-amperes, after being stabilized well before the measurement. The observed values are shown in Fig. 5, together with the calculated ones. The calculation of $\mu(E)$ was performed according to the International Tables.[16] A good agreement was obtained except in the high-energy region and the low-energy region. In the former region, the calculated absorption coefficients are somewhat smaller than the observed ones, while in the latter region, the calculated absorption coefficients are larger. The observed absorption coefficients were used for the data analysis.

In the present work, the transmission geometry is adopted and the absorption factor $A_{coh}(E,\theta)$ is given simply by

$$A_{coh}(E,\theta) = \exp(-\mu(E) l \sec\theta), \quad (6)$$

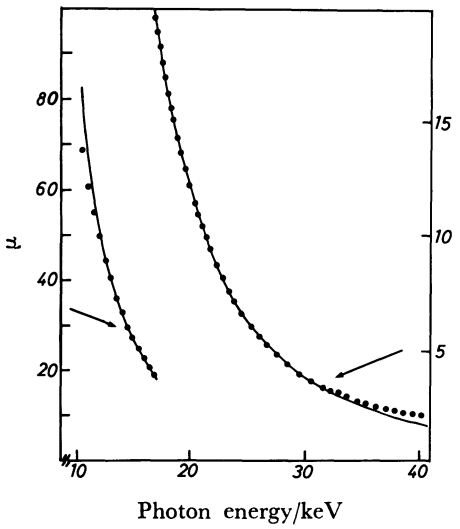

Fig. 5. The observed (dots) and calculated (solid curve) linear absorption coefficient, μ, of liquid CCl_4.

where l is the thickness of the sample.[2] The incoherent absorption factor $A_{inc}(E,E',\theta)$ is given by

$$A_{inc}(E,E',\theta) = \int_0^l \exp[-\mu(E)x\sec\theta - \mu(E')(l-x)\sec\theta]dx/l$$
$$= \frac{\exp(-\mu(E')l\sec\theta)}{l\mu(E)\sec\theta(1-\mu(E')/\mu(E))} \times [1-\exp\{-\mu(E)l\sec\theta(1-\mu(E')/\mu(E))\}], \quad (7)$$

if Compton scattering is assumed to occur with equal probability at any place inside the sample.

Egami proposed the reflection geometry as the optical system,[7] because the absorption factor $A(E,\theta)$ is proportional to $\mu(E)^{-1}$ in this arrangement. However, this is valid only when the incident beam is completely absorbed by the sample and when all the X-rays scattered at a particular angle from the sample are collected by the detector. In order to satisfy these conditions, it is necessary to use a wide detector slit on the side of the sample. This results in loss of angular resolution, which causes a serious error, as mentioned in the section of the slit correction. Moreover, the reflection geometry makes it difficult to measure scattering intensities at low angles.

Problems in the Scattering Process

Multiple Scattering. We have considered the kinematical double scattering, following the method by Warren and Mozzi,[17] who reported the correction for the double scattering of an amorphous sample in the case of reflection geometry and for the angle-dispersive method. We have calculated the effect of the double scattering for the transmission geometry and for the used region of the photon energy. The details are given in Appendix 2. In the case of the reflection method, Warren and Mozzi[17] and Egami[7] reported that the ratio of the double scattering intensity to the single scattering intensity amounts to 8% and 10%, respectively. However, in the case of transmission method, the maximum value of this ratio is 1.5%. This is because the sample is very thin (0.5 mm in the present experiment) in the transmission method. The energy-dependence of the ratio is rather small, but the ratio becomes larger as the scattering angle increases, as is shown in Appendix 2 (Fig. 13).

Compton Scattering. In the energy-dispersive method, the observed intensities are the sum of the intensities of incoherent scattering or Compton scattering and coherent scattering. The accumulated counts at a certain channel corresponding to the photon energy E contain the counts of incoherently scattered photons which have the incident energy E'. E' is larger than E by the Compton shift ΔE, which is given by

$$\Delta E = \frac{2E^2\sin^2\theta}{mc^2} \frac{1}{\left(1-\frac{2E}{mc^2}\sin^2\theta\right)}. \quad (8)$$

Since it is difficult to measure the incoherent scattering of the sample separately, we used the sum of

atomic incoherent scattering factors of the constituent atoms for the stoichiometric unit of the sample, denoted by I_{inc} multiplied by the recoil factor K, in the analysis. The atomic incoherent scattering factors are calculated by Cromer.[18] The Breit-Dirac recoil factor K is $(E/E')^2$ in the case of free electrons, and the ratio of the band width, $(dE'/dE)=(E'/E)^2$, cancels out the recoil factor, as pointed out by Egami[3] (see Eq. 9). However, for a system with bound electrons, the recoil factor is (E/E'),[19] and accordingly the product $K(dE'/dE)$ becomes (E'/E). Compton scattering has a profile with a width due to the momentum distribution of electrons, but it is permissible to neglect this width in the analysis.

Reduction to the Structure Function

After we measured the energy spectrum of X-rays from the sample, the structure function is obtained according to the following processes.

First the escape correction and the slit correction are performed. After these corrections, the observed spectrum $I_{obsd}(E,\theta)$ is expressed as

$$\begin{aligned} I_{obsd}(E,\theta) = k[&A_{coh}(E,\theta)P(E,\theta)I_p(E)I_{coh}(E,\theta) \\ &+ K(dE'/dE)A_{inc}(E,E',\theta)P(E',\theta)I_p(E')I_{inc}(E',\theta) \\ &+ A_{coh}(E,\theta)P(E,\theta)I_p(E)D(E,\theta)] \\ &+ A_{coh}(E,\theta)I_{back}(E,\theta) \end{aligned} \quad (9)$$

In Eq. 9, A is the absorption factor, P the polarization factor, I_{coh} and KI_{inc} are the coherent and incoherent scattering intensities of the sample, respectively. D is the double scattering intensity. I_{back} is the experimentally obtained background intensity, which includes the scattering from windows of the sample holder and that from air, and the intensity of parasitic scattering. $I_p(E)$ is the energy spectrum of the primary beam, obtained experimentally as mentioned in previous Chapter, including the attenuation due to the X-ray absorption by air and the detector efficiency. For I_p and I_{back} described in Eq. 9, the escape correction and the slit correction are already performed. The scale factor k normalizes the observed intensity to the absolute scale of the stoichiometric unit of the liquid. E' is the initial photon energy which is reduced to E after Compton scattering. The polarization factor, P, in Eq. 9 is given by

$$P(E,\theta) = (1+\cos^2 2\theta)/2 + (1-\cos^2 2\theta)\Pi(E)/2, \quad (10)$$

in terms of the polarization $\Pi(E)$, which has been determined experimentally as mentioned in the previous section.

Second, with the use of the absorption factor $A_{coh}(E,\theta)$ calculated by the use of the measured values of $\mu(E)$ and Eq. 6, the fourth term in Eq. 9 is subtracted easily. Dividing the remaining term by the factor $A_{coh}(E,\theta)P(E,\theta)I_p(E)$, we obtain the following quantity:

$$\begin{aligned} I'_{obsd}(E,\theta) = k\Big\{&I_{coh}(E,\theta) + \frac{(E'/E)A_{inc}(E,E',\theta)P(E',\theta)I_p(E')}{A_{coh}(E,\theta)P(E,\theta)I_p(E)} \\ &\times I_{inc}(E',\theta) + D(E,\theta)\Big\} \end{aligned} \quad (11)$$

The product $K(dE'/dE)$ has been replaced by (E'/E) as discussed in the preceding section. All the factors in the second term in Eq. 11 are known. The double scattering intensity, $D(E,\theta)$ has been estimated as described in Appendix 2.

Next, we should determine the scale factor k as in the following process. The total coherent intensity I_{coh} is composed of three terms; that is,

$$I_{coh}(E,\theta) = \sum_n f_n(s)^2 + i_1 + i_2 \quad (12)$$

where the first term is the self-scattering intensity from the constituent atoms, the second term i_1 represents the molecular term which is the result of the interference from each atom pair within a molecule, and the third term i_2 represents the interference from atom pairs between different molecules. Since the term i_2 in Eq. 12 vanishes at large s-values, I_{coh} is given by the first and second terms in Eq. 12. The scale factor k to normalize the experimental intensity to the absolute intensity is obtained by comparing the experimental intensity with the calculated absolute intensity, which is composed of I_{coh} and the second and third terms in Eq. 11. The scale factor k was easily obtained for the data at 2θ=28, 40, and 56°.

For the data which are obtained at smaller scattering angles, the approximation of $i_2 \simeq 0$ is not valid. Utilizing the values of $I_{coh}(s)$ obtained by the data at 2θ=28° for the overlapping s-region of 2θ=28° and the next lower angle 2θ=16°, we can calculate the absolute intensity for 2θ=16°, because $I_{coh}(E,\theta)$ is simply a function of s, and the second and the third terms of Eq. 11 are known. By comparing the calculated absolute intensity and $I'_{obsd}(E,2\theta=16°)$, the scale factor k for 2θ=16° is determined. This procedure is repeated for the data obtained at lower scattering angles, and both k and $I_{coh}(s)$ can be determined.

The obtained total coherent intensity $I_{coh}(s)$ for liquid CCl_4 at room temperature is shown in Fig. 6 by a solid curve, together with the calculated values of the self-scattering intensity from the individual atoms, *i.e.*, $\sum_n f_n(s)^2$ by broken curve. The weighted structure function, $si(s)$, is shown in Fig. 7, where $i(s)$

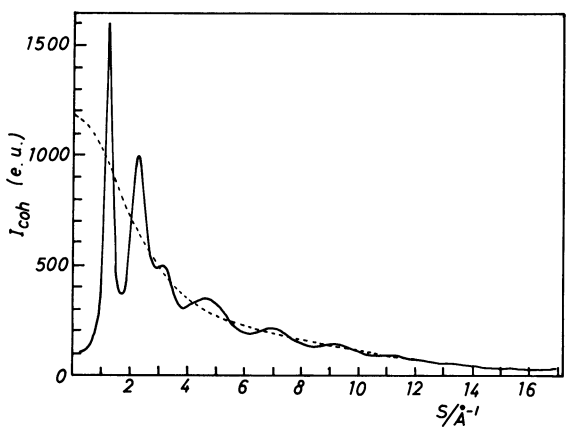

Fig. 6. The observed total coherent intensity $I_{coh}(s)$ for liquid CCl_4 (solid curve) and self-scattering intensity from the constituent atoms (broken curve).

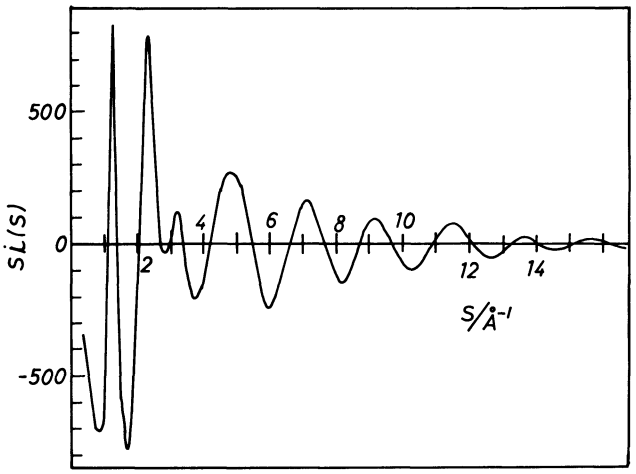

Fig. 7. Weighted structure function $si(s)$ for liquid CCl_4 at room temperature.

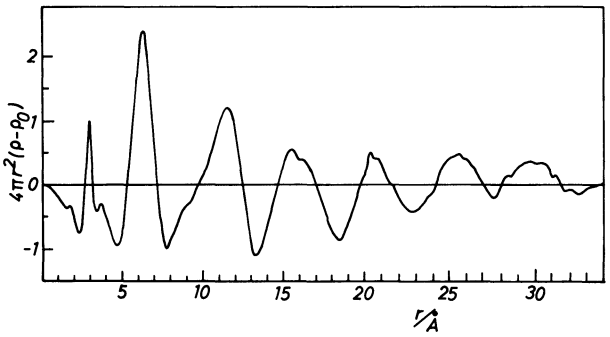

Fig. 8. The electronic distribution function of liquid CCl_4 containing the distribution of electron cloud, $4\pi r^2(\rho-\rho_0)$.

is the reduced intensity defined by

$$i(s) = I_{\text{coh}} - \sum_n f_n(s)^2 = i_1 + i_2. \quad (13)$$

The weighted structure function contains the information on the molecular structure and on the arrangement of molecules in the liquid.

The distribution function containing the distribution of electron cloud is shown in Fig. 8. It is defined by the Fourier transform of the weighted structure function, $si(s)$,

$$4\pi r^2(\rho-\rho_0) = \frac{2r}{\pi\sum_n Z_n^2}\int si(s)\sin sr ds, \quad (14)$$

where ρ_0 is the bulk number density of the liquid and Z_n is the atomic number of the n-th component atom.

Discussion

We have enumerated many factors which affect the accuracy of the intensity data obtained by the energy-dispersive method and taken them into account in the analysis. Whether or not the corrections have improved the experimental results is ascertained in the following two ways. First, we can check the consistency of the data in the same s-region which

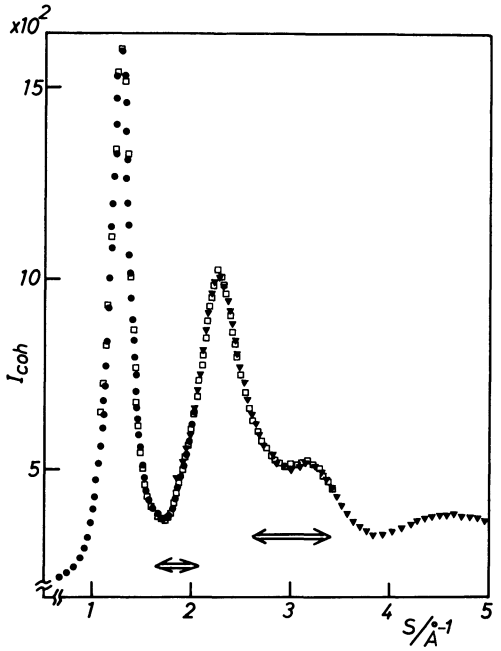

Fig. 9. The total coherent intensity for liquid CCl_4 to show the consistency of the data obtained by different angle-setting. The marks such as ●, □, and ▼ show the data obtained by the angle-setting at $2\theta = 6$, 10, and 16°, respectively. The arrows show the region used for determining the scale factor k.

are collected at different scattering angles and analyzed independently. This consistency is very good as is shown in Fig. 9, when the energy region ranging from 10 to 38 keV is used. In the energy region lower than 10 keV, the absorption by liquid is very strong, and the uncertainty of the observed transmittance becomes large. In the energy region higher than 38 keV, the uncertainty of the polarization of the primary beam becomes large. In the case of liquid CCl_4, the energy region of 10—38 keV is suitable to use for the measurement of scattering intensities.

Second, in order to evaluate the procedure of the present work, the intensity data obtained by the present experiment may be compared with data obtained by the angle-dispersive method. The diffraction intensity of this sample (liquid CCl_4) has been measured by several authors.[20-23] However, only Narten presented the numerical values of the intensity data in the table.[23] Our experiment has been carried out at room temperature and Narten reported the data at 20°C. So, our data obtained by energy-dispersive method have been compared with those of Narten in the form of the molecular structure function $H(s)$, where $H(s)$ is defined by

$$H(s) = i(s)/(\sum_n f_n(s))^2. \quad (15)$$

As is shown in Fig. 10, the present structure function is in fairly good agreement with the one by Narten[23] except for the small s-region. In Fig. 10, our data are shown by a solid curve and Narten's data by dots. A large difference is observed at the small s-region (s= 0—1.3 Å^{-1}). For the region of s less than 1 Å^{-1}, the values of $H(s)$ by Narten are too small, because for

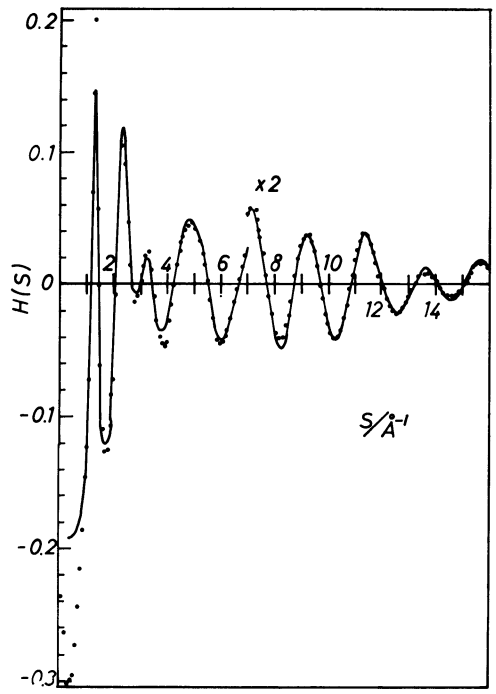

Fig. 10. The comparison of the structure function $H(s)$ of the present work and Narten's.[23] Solid curve is the present data and dots show Narten's.

liquid CCl_4 the structure function $H(s)$ can never be less than -0.217, even if the total coherent intensity I_{coh} were equal to zero at $s\simeq 0$ Å^{-1}. For the peak-height at $s\simeq 1.3$ Å^{-1}, Narten's value is much higher than our data. We can not understand why these discrepancies in $H(s)$ exist in the small s-region, because the total coherent intensity obtained by Narten[23] shows very good agreement with ours (Fig. 6) in the region $s\simeq 0$ Å^{-1} and also for the peak-height at $s\simeq 1.3$ Å^{-1}.

The results mentioned above seem to show the need of the corrections discussed in the present paper.

The diffraction intensity of liquid CCl_4 was also measured as the first sample when Murata and Nishikawa constructed an energy-dispersive diffractometer.[2] The main difference between the previous and the present data is the peak-height of the first peak at $s\simeq 1.3$ Å^{-1}. The first peak of the present data is much higher than that of the previous data, because in the previous analysis the slit correction was not made. In the data corrections which we have newly made, the effect of the slit correction is the largest. Especially for liquid CCl_4, whose diffraction pattern has a very sharp peak at small s-region, the divergence of the scattering angle in the experimental condition is very sensitive to the peak-height.

We believe that solutions have been given to the problems in the analysis of the diffraction data obtained by the energy-dispersive method. One of the remaining problems may be the anomalous dispersion. In the case of CCl_4, this effect is rather small in the energy range used in the experiment. However, this effect should be taken into account for samples containing heavier atoms.

By the revision and improvement of the analysis for the data obtained by the energy-dispersive method, the intensity data of liquid CCl_4 have been improved, but the structure model is unchanged. The model of the bcc local structure[24] has turned out to be still valid with better agreement between the observed and the simulated curves of the structure function. The discussion on the structure of liquid CCl_4 will be reported in detail in a succeeding paper.

The authors wish to express their thanks to Messrs. Masayoshi Hamano, Hiroshi Miyagi, and Yuzi Shimokawa of the machine shop of Gakushuin University for the construction of the vertical tube holder to measure the polarization of the primary beam. Their thanks are also due to Professor Hideki Morikawa of Tokyo Institute of Technology for offering the sample of silica glass. The present work is a continuation to the research project initiated by Professor Yoshitada Murata of the Institute for Solid State Physics, the University of Tokyo.

Appendix 1

Slit Correction. For middle or large angle scattering experiments, the widths of the slits which are ordinarily used have a smearing effect on the observed intensity data. It is also permissible to neglect the effect of the finite slit height. We describe the slit correction for the diffraction data which are smeared due to the width of the slits.

The experimental scattered intensity $\tilde{I}(E,\theta)$ for a scattering angle 2θ is related to the scattered intensity of the perfect collimation, $I(E,\theta)$, by the equation

$$\begin{aligned}\tilde{I}(E,\theta) &= \iiint I(E,\theta+\delta\theta)W(w,z,u)\mathrm{d}w\mathrm{d}z\mathrm{d}u \\ &\quad / \iiint W(w,z,u)\mathrm{d}w\mathrm{d}z\mathrm{d}u \\ &= \iiint [I(E,\theta)+I'(E,\theta)\delta\theta+\tfrac{1}{2}I''(E,\theta)\delta\theta^2] \\ &\quad \times W\mathrm{d}w\mathrm{d}z\mathrm{d}u / \iiint W\mathrm{d}w\mathrm{d}z\mathrm{d}u. \qquad \text{(A1.1)}\end{aligned}$$

where $W(w,z,u)$ is a weight function, the form of which depends on the collimation system. The parameters w, z, and u are the deviations of a path of X-rays from the central line (chained line in Fig. 11) in the collimator, on the side of the incident slit, on the sample and on the detector slit, respectively, as is shown in Fig. 11. The central lines

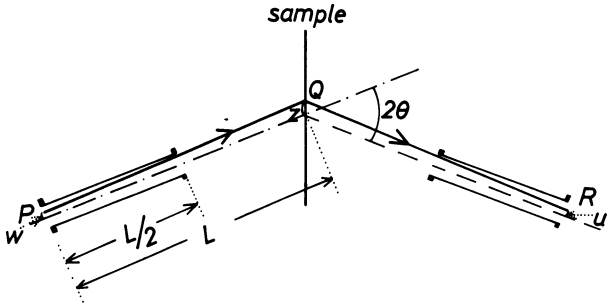

Fig. 11. Geometry of the slit system. We consider the angle dispersion for the X-rays which pass through P, Q and R.

determine the scattering angle 2θ. The notations I' and I'' show the first and second derivatives of the intensity I. In Eq. A1.1, the angular deviation $\delta\theta$ is a function of w, z, and u. Equation A1.1 is rewritten as

$$\tilde{I}(E,\theta) = I(E,\theta) + I'(E,\theta)\iiint \delta\theta W \mathrm{d}w\mathrm{d}z\mathrm{d}u \Big/ \iiint W \mathrm{d}w\mathrm{d}z\mathrm{d}u + \frac{1}{2}I''(E,\theta)\iiint \delta\theta^2 W \mathrm{d}w\mathrm{d}z\mathrm{d}u \Big/ \iiint W \mathrm{d}w\mathrm{d}z\mathrm{d}u \quad \text{(A1.2)}$$

The second term in Eq. A1.2 vanishes, because it is possible to assume that the function $(\delta\theta W)$ is an odd function of the parameters w, z, and u. Let us define the angle dispersion ξ by the following relation:

$$\xi = (\overline{\delta\theta^2})^{1/2} = \left[\iiint \delta\theta^2 W \mathrm{d}w\mathrm{d}z\mathrm{d}u \Big/ \iiint W \mathrm{d}w\mathrm{d}z\mathrm{d}u\right]^{1/2}. \quad \text{(A1.3)}$$

We have

$$\tilde{I}(E,\theta) = I(E,\theta) + \frac{1}{2}I''(E,\theta)\xi^2. \quad \text{(A1.4)}$$

On the other hand,

$$\tilde{I}(E,\theta+\xi) = \tilde{I}(E,\theta) + \tilde{I}'(E,\theta)\xi + \frac{1}{2}\tilde{I}''(E,\theta)\xi^2 \quad \text{(A1.5)}$$

$$\tilde{I}(E,\theta-\xi) = \tilde{I}(E,\theta) - \tilde{I}'(E,\theta)\xi + \frac{1}{2}\tilde{I}''(E,\theta)\xi^2 \quad \text{(A1.6)}$$

By the summation of Eq. A1.5 and Eq. A1.6, we obtain

$$\tilde{I}''(E,\theta)\xi^2 = \tilde{I}(E,\theta+\xi) + \tilde{I}(E,\theta-\xi) - 2\tilde{I}(E,\theta). \quad \text{(A1.7)}$$

Now, we make an appriximation,

$$\tilde{I}''(E,\theta) = I''(E,\theta), \quad \text{(A1.8)}$$

then we have

$$I(E,\theta) = 2\tilde{I}(E,\theta) - \frac{1}{2}[\tilde{I}(E,\theta+\xi)+\tilde{I}(E,\theta-\xi)], \quad \text{(A1.9)}$$

from Eq. A1.4 and Eq. A1.7. This equation corresponds to Eq. 4 in the text. With enough accuracy, we can approximate the intensity $\tilde{I}(E,\theta+\xi)$ by $\tilde{I}(E+\delta E,\theta)$, where the pair of parameters $E+\delta E$ and θ gives the same s-value as the pair of E and $\theta+\xi$.

The angle dispersion must be estimated for a particular optical geometry. Let us consider a path of X-rays which pass through the points P, Q, and R (see Fig. 11). Let the incident collimator be placed symmetrically to the detecting collimator. For low scattering angles, we have

$$\delta(2\theta) = (z-w)/L + (z-u)/L$$

or

$$\delta\theta = [2z-(w+u)]/2L \quad \text{(A1.10)}$$

where L is the distance between the slit on the side of the X-ray tube (or the detector) and the sample, and $\cos\theta$ is approximated by unity. For the gentle peaks obtained at large scattering angles, the angle dispersion causes little smearing effect. We consider the slit correction only for the case of low scattering angles. Let us derive the expressions of ξ for some optical systems.

Case 1: The incident beam is perfectly parallel and u is fixed to zero. In this case,

$$\delta\theta = z/2L$$
$$W(w,z,u)\mathrm{d}w\mathrm{d}z\mathrm{d}u = Q(z)\mathrm{d}z.$$

where $Q(z)$ is simply a constant for the slit system, and is given by

$$Q(z) = 1/2d. \quad \text{(A1.11)}$$

Accordingly,

$$\xi^2 = \int_{-d}^{d}\left(\frac{z}{2L}\right)^2\frac{1}{2d}\mathrm{d}z \Big/ \int_{-d}^{d}\left(\frac{1}{2d}\right)\mathrm{d}z = d^2/12L^2 \quad \text{(A1.12)}$$

Case 2: The incident beam is perfectly parallel and u is not fixed to zero. This case gives the following relations:

$$\delta\theta = (z-u)/2L$$
$$W(w,z,u)\mathrm{d}w\mathrm{d}z\mathrm{d}u = V(z,u)\mathrm{d}z\mathrm{d}u$$

where

$$\text{if } |z| \geq |u|, \quad \text{then } V(z,u) = Q(z)$$

and

$$\text{if } |z| < |u|, \quad \text{then } V(z,u) = Q(u).$$

Considering the symmetrical property of the beam around the central lines, we can omit the cross term of u and z, and we have

$$\begin{aligned}\xi^2 &= \iint\left(\frac{z-u}{2L}\right)^2 V(z,u)\mathrm{d}z\mathrm{d}u \Big/ \iint V(z,u)\mathrm{d}z\mathrm{d}u \\ &= \frac{1}{4L^2}\iint(z^2+u^2)V(z,u)\mathrm{d}z\mathrm{d}u \Big/ \iint V(z,u)\mathrm{d}z\mathrm{d}u \\ &= \frac{1}{4L^2}\left\{2\left[\int_{z=0}^{d}\int_{u=0}^{z}\left(\frac{z^2+u^2}{2d}\right)\mathrm{d}u\mathrm{d}z + \int_{u=0}^{d}\int_{z=0}^{u}\left(\frac{z^2+u^2}{2d}\right)\mathrm{d}z\mathrm{d}u\right]\right. \\ &\quad \left./2\left[\int_{z=0}^{d}\int_{u=0}^{z}\mathrm{d}uQ(z)\mathrm{d}z + \int_{u=0}^{d}\int_{z=0}^{u}\mathrm{d}zQ(u)\mathrm{d}u\right]\right\} \\ &= d^2/6L^2 \end{aligned} \quad \text{(A1.13)}$$

Case 3: Let the length of the collimator be L; namely, there is no separation between the collimators and the sample. In this case, we find

$$\delta\theta = [2z-(\omega+u)]/2L$$
$$W(w,z,u)\mathrm{d}w\mathrm{d}z\mathrm{d}u = Q(q)\mathrm{d}w\mathrm{d}z\mathrm{d}u$$

where q is the maximum among $|u|$, $|z|$, and $|w|$. By the same reason as in Case 2, the cross terms of w, z, and u vanish, and we obtain the following relation:

$$\begin{aligned}\xi^2 &= \iiint\left[\frac{2z-(w+u)}{2L}\right]^2 Q(q)\mathrm{d}w\mathrm{d}z\mathrm{d}u \Big/ \iiint Q(q)\mathrm{d}w\mathrm{d}z\mathrm{d}u \\ &= \frac{1}{4L^2}\iiint(4z^2+w^2+u^2)Q(q)\mathrm{d}w\mathrm{d}z\mathrm{d}u \\ &\quad \Big/ \iiint Q(q)\mathrm{d}w\mathrm{d}z\mathrm{d}u.\end{aligned}$$

The integration can be analytically performed to give

$$\xi^2 = d^2/2L^2 \quad \text{(A1.14)}$$

Case 4: In the optical geometry of the present work the length of the collimator is $L/2$. In this most realistic case,

$$\delta\theta = [2z-(w+u)]/2L$$
$$W(w,z,u)\mathrm{d}w\mathrm{d}u\mathrm{d}z = Q(q)\mathrm{d}w\mathrm{d}z\mathrm{d}u$$

where q is the maximum among $|w|$, $|w+z|/2$, $|u+z|/2$, and $|u|$. By the consideration of the symmetrical property of W, the region of the integration is reduced to

$$-d \leq w \leq d,$$
$$0 \leq u \leq d,$$

and

$$-3d \leq z \leq 2d.$$

TABLE 1. THE MEAN SQUARES OF ANGLE DISPERSION, ξ^2, FOR SLIT AND APERTURE SYSTEMS

L is the distance between the detector and the sample. The notations d and r refer to half of the slit width and the radius of the aperture, respectively.

	Slit	Aperture
Case 1	$d^2/12L^2$	$r^2/16L^2$
Case 2	$d^2/6L^2$	$2r^2/15L^2$
Case 3	$d^2/2L^2$	$5r^2/12L^2$
Case 4	$1.706\times d^2/L^2$	$1.404\times r^2/L^2$

In this case, we can not integrate Eq. A1.3 analytically. The result obtained by numerical integration is

$$\xi^2 = \iiint\left[\frac{2z-(w+u)}{2L}\right]^2 Q(q)\mathrm{d}w\mathrm{d}z\mathrm{d}u \Big/ \iiint Q(q)\mathrm{d}w\mathrm{d}z\mathrm{d}u = 1.706\times d^2/L^2 \quad \text{(A1.15)}$$

For the aperture systems with the radius r, the weight function becomes

$$Q_A(x) = 2\sqrt{r^2-x^2}/\pi r^2 \quad \text{(A1.16)}$$

in place of Eq. A1.11, and ξ^2 can be calculated by replacing $Q(x)$ by $Q_A(x)$. For comparison, the expressions of ξ^2 for both slit systems and aperture systems are listed in Table 1, for cases 1 to 4.

Appendix 2

Multiple scattering. The following calculation was made with reference to the work by Warren and Mozzi.[17] Let us consider the double scattering from the sample for the transmission geometry. The power of the primary beam is given by I_0S_0, where I_0 is the intensity of the primary beam per unit area and S_0 is the cross section area of the primary beam. Let n be the number density of the units of composition, and $J(2\theta)$ be the intensity of the single scattering per unit of composition for the scattering angle 2θ. Let $\mathrm{d}I_r$ be the intensity at distance r from the volume element $\mathrm{d}V_1$ due to the scattering of the primary beam by $\mathrm{d}V_1$, then

$$\mathrm{d}I_r = A_1P_1I_0\frac{e^4}{m^2c^4r^2}J(2\theta_1)nS_0\mathrm{d}t \quad \text{(A2.1)}$$

where A_1 is the absorption factor, P_1 the polarization factor and r is the distance between volume element $\mathrm{d}V_1$ and $\mathrm{d}V_2$. Let $\mathrm{d}I(2)$ be the intensity at the point of observation at distance R from the sample, due to the scattering of the intensity $\mathrm{d}I_r$ by the volume element $\mathrm{d}V_2$.

$$\mathrm{d}I(2) = A_2P_2\mathrm{d}I_r\frac{e^4}{m^2c^4R^2}J(2\theta_2)n\mathrm{d}V_2. \quad \text{(A2.2)}$$

Here, the volume element $\mathrm{d}V_2$ is given by

$$\mathrm{d}V_2 = r^2\cos\varepsilon\mathrm{d}\varepsilon\mathrm{d}\varphi\mathrm{d}r, \quad \text{(A2.3)}$$

(see Fig. 12 for the definitions of the angles θ, $2\theta_1$, $2\theta_2$, ε, and φ and of the distances t and r). By Eq. A2.1 for $\mathrm{d}I_r$, we have

$$\mathrm{d}I(2) = I_0S_0AP\left(\frac{e^4}{m^2c^4}\right)^2\frac{n^2}{R^2}J(2\theta_1)J(2\theta_2)\cos\varepsilon\,\mathrm{d}\varepsilon\mathrm{d}\varphi\mathrm{d}t\mathrm{d}r. \quad \text{(A2.4)}$$

The absorption factor A in Eq. A2.4 is given by

$$A = \exp(-\mu f(r))$$

where μ is the linear absorption coefficient and $f(r)$ is the path length of the X-ray beam in the sample and given by

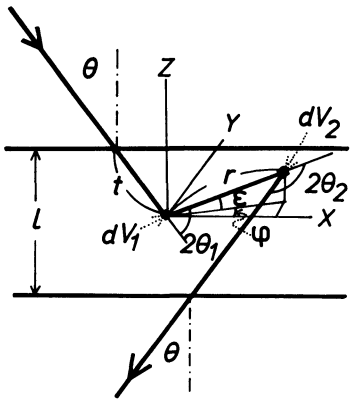

Fig. 12. Geometry of the double scattering process for the transmission method.

$$f(r) = r + l/\cos\theta + r\sin\varepsilon/\cos\theta \quad \text{(A2.5)}$$

where l is the thickness of the sample. The polarization factor P is given by

$$P = \cos^2 2\theta_1 + \cos^2 2\theta_2 + (\cos 2\theta_1\cos 2\theta_2 - \cos 2\theta)^2/2. \quad \text{(A2.6)}$$

The polarization of the primary beam is neglected, because it is small in the energy region we used. The double scattering $I(2)$ is given by the integration of Eq. A2.4 by the parameters t, r, ε, and φ.

First let us consider the integration by the parameters t and r. In the integrand in Eq. A2.4 only the absorption factor A is a function of the parameters t and r. We define A' by

$$A' = \iint \exp(-\mu f(r))\mathrm{d}r\mathrm{d}t.$$

The region of the integration by r for the case of forward scattering ($\varepsilon\leq 0$) is different from that for back scattering ($\varepsilon>0$). For the former, r goes from 0 to $(l-t\cos\theta)/(-\sin\varepsilon)$ and for the latter, r goes from 0 to $t\cos\theta/\sin\varepsilon$. The region of the integration for t is the same for the two cases and becomes from 0 to $l\sec\theta$. For the forward scattering, we obtain

$$A' = \int_{t=0}^{l\sec\theta}\int_{r=0}^{\frac{-l+t\cos\theta}{\sin\varepsilon}} \exp\{-\mu f(r)\}\mathrm{d}r\mathrm{d}t = \exp(-\mu l\sec\theta)\left[\frac{\cos\theta\cdot\sin\varepsilon}{\mu^2(\cos\theta+\sin\varepsilon)^2} \times\{1-\exp[\mu l(\sec\theta+\mathrm{cosec}\,\varepsilon)]\}+\frac{l}{\mu(\cos\theta+\sin\varepsilon)}\right] \quad \text{(A2.7)}$$

For the back scattering, we have

$$A'' = \int_{t=0}^{l\sec\theta}\int_{r=0}^{\frac{t\cos\theta}{\sin\varepsilon}} \exp\{-\mu f(r)\}\mathrm{d}r\mathrm{d}t = \exp(-\mu l\sec\theta)\left[\frac{\cos\theta\sin\varepsilon}{\mu^2(\cos\theta+\sin\varepsilon)^2} \times\{\exp[-\mu l(\sec\theta+\mathrm{cosec}\,\varepsilon)]-1\}+\frac{l}{\mu(\cos\theta+\sin\varepsilon)}\right] \quad \text{(A2.8)}$$

Next, we relate the scattering angles $2\theta_1$ and $2\theta_2$ to the angles θ, ε, and φ. By a simple calculation, we obtain

$$\cos 2\theta_1 = \cos\varepsilon\cos\varphi\sin\theta - \sin\varepsilon\cos\theta$$

and

$$\cos 2\theta_2 = -\cos\varepsilon\cos\varphi\sin\theta - \sin\varepsilon\cos\theta. \quad \text{(A2.9)}$$

We have

$$I(2) = I_0 S_0 \left(\frac{e^4}{m^2c^4}\right)^2 \frac{n^2}{R^2} \times \left[\int_{\varphi=-\pi}^{\pi}\int_{\varepsilon=-\frac{\pi}{2}}^{0} A'\cdot P\cdot J(2\theta_1)J(2\theta_2)\cos\varepsilon\, d\varepsilon d\varphi + \int_{\varphi=-\pi}^{\pi}\int_{\varepsilon=0}^{\frac{\pi}{2}} A''\cdot P\cdot J(2\theta_1)J(2\theta_2)\cos\varepsilon\, d\varepsilon d\varphi\right]$$
$$= I_0 S_0 \left(\frac{e^4}{m^2c^4}\right)^2 \frac{n^2}{R^2} \times 2\left[\int_{\varphi=0}^{\pi}\int_{\varepsilon=\frac{\pi}{2}}^{0} A'\cdot P\cdot J(2\theta_1)J(2\theta_2)\cos\varepsilon\, d\varepsilon d\varphi + \int_{\varphi=0}^{\pi}\int_{\varepsilon=0}^{\frac{\pi}{2}} A''\cdot P\cdot J(2\theta_1)J(2\theta_2)\cos\varepsilon\, d\varepsilon d\varphi\right] \quad \text{(A2.10)}$$

On the other hand, the corresponding intensity of the single scattering is given by

$$I(1) = I_0\left(\frac{e^4}{m^2c^4}\right)\frac{nl\sec\theta S_0}{R^2}\left(\frac{1+\cos^2\theta}{2}\right)J(2\theta)\exp(-\mu l\sec\theta) \quad \text{(A2.11)}$$

The double scattering ratio to the single scattering is $I(2)/I(1)$ and is calculated by Eq. A2.10 and A2.11. In the calculation of Eq. A2.10, numerical integration is made for the parameters ε and φ. The intensity $J(2\theta)$ (and $J(2\theta_1)$, $J(2\theta_2)$) is approximated by

$$J(2\theta) = \sum_n f_n(E,\theta)^2 + I_{inc}(E,\theta). \quad \text{(A.12)}$$

This approximation is good enough because the double scattering is averaged over all directions and shows a smooth change for the scattering parameter s.

For each energy used for the experiment, we have calculated the ratio of the double scattering intensity to the single scattering intensity. The result is shown in Fig. 13 for the scattering angles 2θ=2.5, 28, and 55°. The double scattering intensity $D(E,\theta)$ in the text is estimated by $(I(2)/I(1))\,J(2\theta)$.

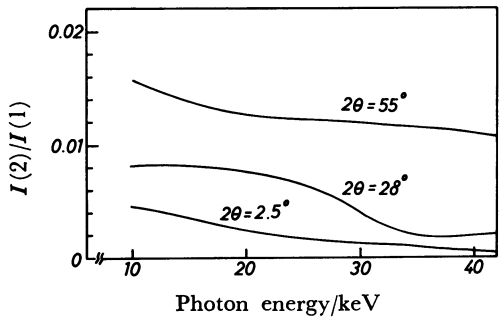

Fig. 13. The double scattering ratios to the single scattering *vs.* photon energies. The ratios are shown for the scattering angles 2θ=2.5, 28, and 55°.

References

1) B. C. Giessen and G. E. Gordon, *Science*, **159**, 973 (1968).
2) Y. Murata and K. Nishikawa, *Bull. Chem. Soc. Jpn .*, **51**, 411 (1978).
3) T. Egami, *J. Mater. Sci .*, **13**, 2587 (1978).
4) T. Egami, *J. Appl. Phys .*, **50**, 1564 (1979).
5) J. M. Prober and J. M. Schultz, *J. Appl. Crystallogr .*, **8**, 405 (1975).
6) T. Iijima and T. Mitsuhashi, "X-ray Instrumentation for Photon Factory," ed by Hosoya, KTK Publishing Co., Tokyo (in press).
7) T. Egami, *Topics in applied Physics* , **46**, 25 (1981).
8) K. Nishikawa and N. Kitagawa, *Bull. Chem. Soc. Jpn .*, **53**, 2804 (1980).
9) J. A. Bearden, *Rev. Mod. Phys.*, **39**, 78 (1967).
10) J. H. Hubbell, Wm. J. Veigele, E. A. Briggs, R. T. Brown, D. T. Cromer, and R. J. Howerton, *J. Phys. Chem. Ref. Data.*, **4**, 471 (1975).
11) A. H. Compton and S. K. Allison, "X-rays in Theory and Experiment," D. Van Nostrand Company, Toronto (1949).
12) J. S. Olsen, B. Buras, and T. Jensen, *Acta Crystallogr .*, **A34**, 84 (1978).
13) T. Fukamachi, S. Togawa, and S. Hosoya, *J. Appl. Crystallogr.*, **6**, 297 (1973).
14) T. Mitsuhashi, J. Nagao, and T. Iijima, Annual Meeting of the Crystallographic Society of Japan, Tokyo (1982).
15) O. Kratky, G. Porod, and Z. Skala, *Acta Phys. Austriaca*, **13**, 76 (1960).
16) "International Tables for X-ray Crystallography," Vol III, Kynoch Press, Birmingham (1962).
17) B. E. Warren and R. L. Mozzi, *Acta Crystallogr.*, **21**, 459 (1966).
18) D. T. Cromer, *J. Chem. Phys.*, **50**, 4857 (1967).
19) R. A. Bonham, *Phys. Rev.*, **A23**, 2950 (1981).
20) R. U. Gruebel and G. T. Clayton, *J. Chem. Phys.*, **46**, 639 (1967).
21) A. H. Narten, M. D. Danford, and H. A. Levy, *J. Chem. Phys.*, **46**, 4875 (1967).
22) G. Reichelt, J. U. Weidner, and W. Zimmermann, *Ber. Bunsenges. Phys. Chem.*, **78**, 1050 (1974).
23) A. H. Narten, *J. Chem. Phys.*, **65**, 573 (1976).
24) K. Nishikawa and Y. Murata, *Bull. Chem. Soc. Jpn.*, **52**, 293 (1979).